FEBS Letters xxx (2010) xxx–xxx

FEBS Letters

journal homepage: www.FEBSLetters.org

Modulation of copper site properties by remote residues determines the stability of plastocyanins

Francisco J. Muñoz-López [a], Estrella Frutos Beltrán [a], Sofía Díaz-Moreno [b], Irene Díaz-Moreno [a], Gloria Subías [c], Miguel A. De la Rosa [a], Antonio Díaz-Quintana [a,*]

[a] Instituto de Bioquímica Vegetal y Fotosíntesis, Universidad de Sevilla y C.S.I.C., Avda. Américo Vespucio 49, 41092 Sevilla, Spain
[b] Diamond Light Source Ltd., Rutherford Appleton Laboratory, Chilton, Didcot, Oxfordshire OX11 0QX, United Kingdom
[c] Instituto de Ciencia de Materiales de Aragón, Universidad de Zaragoza y C.S.I.C., Departamento de Física de la Materia Condensada, Plaza San Francisco s/n, 50009 Zaragoza, Spain

ARTICLE INFO

Article history:
Received 22 December 2009
Revised 7 April 2010
Accepted 7 April 2010
Available online xxxx

Edited by Stuart Ferguson

Keywords:
Protein stability
Metal site stability
Blue copper protein
Plastocyanin
Protein matrix
X-ray absorption spectroscopy

ABSTRACT

The metal cofactor determines the thermal stability in cupredoxins, but how the redox state of copper modulates their melting points remains unknown. The metal coordination environment is highly conserved in cyanobacterial plastocyanins. However, the oxidised form is more stable than the reduced one in thermophilic *Phormidium*, but the opposite occurs in mesophilic *Synechocystis*. We have performed neutral amino-acid substitutions at loops of *Phormidium* plastocyanin far from the copper site. Notably, mutation P49G/G50P confers a redox-dependent thermal stability similar to that of the mesophilic plastocyanin. Moreover, X-ray absorption spectroscopy reveals that P49G/G50P mutation makes the electron density distribution at the oxidised copper site shift towards that of *Synechocystis* plastocyanin.

1. Introduction

Up to a 30% of proteins in living cells contain metal cofactors [1] that affect their stability [2–5] according to their oxidation state, and by mechanisms that are not fully understood yet. The simplicity of the metal cofactor of blue copper proteins (BCPs) makes them an ideal case study to tackle this issue. These proteins show a typical immunoglobulin-like topology in which copper is bound at least by three residues [6]. Among them stands out the photosynthetic electron carrier plastocyanin (Pc) [7,8]. In Pcs, the copper atom is bound by two histidine nitrogen atoms, one cysteine sulfur atom and, more weakly, a methionine sulfur atom. The four ligands set up into a distorted tetrahedral geometry [9,10].

The copper site determines the thermal stability of BCPs [11–13]. In fact, the melting points (T_m) are much lower in apo-BCPs than in the corresponding holoproteins, in which disruption of the copper site precedes unfolding. Moreover, the redox state of the metal modulates their thermal stability. In fact, oxidised species of azurin [4], rusticyanin [14], and Pc from thermophilic cyanobacteria [15] are more thermally stable than the reduced ones, whereas the opposite occurs in Pc from plants [16–18] or non-thermophilic cyanobacteria [19]. Notably, the T_m values of oxidised species span in a range of 20° among organisms, whereas those of the reduced forms vary in a range of only 10° [15–19].

The different effects of the redox state on the stabilities of Pcs were unexpected as all Pcs have the same copper ligands. In cyanobacteria, their sequences show ca 60% identity and the surroundings of the metal site are the most conserved parts of the protein. To tackle this issue, we have performed site-directed mutagenesis of the *pet*E gene coding Pc from the thermophilic cyanobacterium *Phormidium laminosum* (*Pho*-WT). Although modified residues lay 20 Å away from the copper site, they reverse the relation between the oxidation state of the metal and the T_m value of the protein. All mutations affect preferentially the oxidised copper site, in agreement with the larger variability of T_m values of oxidised species among Pcs.

2. Materials and methods

2.1. DNA Techniques

The *pet*E gene, coding for *P. laminosum* Pc [20], was kindly provided by Dr. B. Schlarb (University of Cambridge, UK) and

* Corresponding author. Tel.: +34 954 489 507; fax: +34 954 460 065.
E-mail address: qzaida@us.es (A. Díaz-Quintana).

0014-5793/$36.00 © 2010 Federation of European Biochemical Societies. Published by Elsevier B.V. All rights reserved.
doi:10.1016/j.febslet.2010.04.013

subcloned in pBSII SK(+) under the control of Lac promoter. Site-directed mutagenesis were performed by using the "Quick Change" method (Stratagen Inc., La Jolla, CA, USA).

2.2. Protein expression and purification

Recombinant proteins from *Phormidium* were over-expressed in *Escherichia coli* K12 strain, and purified as reported previously, with minor modifications [15]. The protein concentration was determined by spectrophotometry using an extinction coefficient at 599 nm of 4.3 mM^{-1} cm^{-1} for the oxidised form of Pc [20]. *Syn*-WT was produced and purified as described by De la Cerda et al. [21].

2.3. Fluorescence spectroscopy

Fluorescence was recorded using a Perkin–Elmer LS-5 fluorimeter. Samples contained 25 μM of protein in 10 mM sodium citrate buffer, pH 6. To avoid oxidation of reduced samples along the experiments, equimolar concentrations of sodium ascorbate were added. The experimental setup and conditions were as described in previous work [15]. Data were fitted to a two-state equilibrium mechanism [22] for protein unfolding to estimate the values for T_m, using the equation of Santoro and Bolen [23] adapted to thermal unfolding processes [24].

2.4. Circular dichroism spectra

Circular dichroism (CD) spectra were recorded with a Jasco J-815 spectrometer in a 1 mm quartz cuvette at 25 °C. To measure in the far-UV region, the samples consisted of 3 μM protein in 2 mM citrate buffer, pH 6.3. The spectra were analysed using CDpro [25]. Samples for measurements in the visible region contained 165 μM Pc in 20 mM citrate buffer, pH 6.0.

2.5. Redox titrations

Redox titrations were performed at room temperature as described previously [26] using a Pt–Ag/AgCl combined electrode (Microelectrodes, Inc.).

2.6. X-ray absorption spectroscopy measurements

The X-ray absorption spectra (XAS) were recorded at the European Synchrotron Radiation Facility (ESRF), a 6 GeV machine operating with a ring current of 200 mA. The Cu K-edge (8979 eV) was measured at beam-line BM29 using a flat Si(1 1 1) double crystal monochromator with an energy resolution of $\sim 8 \times 10^{-5}$. 1 mM samples were prepared for this purpose in 5 mM phosphate buffer, pH 7.0 and 40% glycerol. All measurements were made at 77 K in fluorescence mode, using a 13-element Canberra solid-state germanium detector. Samples were loaded into an aluminium 5754 cell with two 12 μm Kapton™ foil windows. To get an internal energy calibration, simultaneous copper foil spectra were acquired in transmission mode, using ionisation chambers as detectors.

For all measurements, each data point was collected along for 4 s, and several scans were averaged to achieve a good signal-to-noise ratio. No photo-reduction or damage of samples was observed, even after several hours of measurement. This was further tested by UV–vis spectroscopy before and after XAS measurements.

Spectra averaging, background subtraction and amplitude normalisation required to obtain the extended X-ray absorption fine-structure (EXAFS) signals (k) were performed using the Athena (version 0.8.058) code [27] The best fit to the data was performed by using the Artemis program (version 0.8.013) [28,29].

3. Results

3.1. Design and characterisation of plastocyanin mutants

To obtain an insight into the factors affecting the different thermal stability behaviour of *Pho*-WT a, regards their thermal stabilities, we have destabilised *Pho*-WT by mutating residues not conserved in *Syn*-WT. *Syn*-WT shows a lower thermal stability at its N-terminus and first β-strand than *Pho*-WT [19]. Phe3 (see Fig. 1) of *Pho*-WT keeps van der Waals contacts Val21 and Val23 at this β-strand, but it is replaced by Ala in *Syn*-WT. Thus, we replaced Phe3 by Ala in *Pho*-WT to make this region more mobile.

A loop region (loop 5) containing a small α-helix, at the opposite protein side, flanks and closes the β-barrel. This region shows a low degree of sequence conservation. Its stability is larger in Pho-WT than in Syn-WT [30]. According to Molecular Dynamics calculations, loop 5 being highly mobile [19,30]. Moreover, non-bonding interactions such as that between Pro49 and Tyr85 (Fig. 1) anchor it to the barrel [30]. Hence, we designed the double substitution P49G/G50P, to prevent this interaction. G50P substitution was introduced in this mutant to assure the smallest effect on the conformational entropy loss upon folding. In fact, a single replacement of Pro49 by a short-side-chain residue might increase much the conformation entropy of the unfolding state. The single mutation P49G was designed but could not be isolated.

Finally, *Pho*-WT has an insertion at loop 7 (See Fig. 1) providing an aromatic residue, Phe80, which contacts Ile55 and Leu59 at loop 5 and Phe76, Pro81 and Tyr85 at the β-barrel. We replaced Phe80 by Ala to loosen its surroundings.

Circular dichroism data indicate that all mutants are folded and have approximately the same secondary structure content as *Pho*-WT: 3.1 ± 1.0% α-helix, 40.0 ± 1.1% β-strand, 22.4 ± 1.2% turns and 33.9 ± 1.4% of non-regular structure. In addition, these mutations hardly affect the redox potential of the protein (321 ± 8 mV) at room temperature. In fact, the values corresponding to F3A, P49G/G50P and F80A were 317 ± 14, 311 ± 10 and 311 ± 6 mV, respectively.

3.2. Melting point determinations

Fig. 2 shows normalised thermal unfolding curves for the oxidised and reduced forms of *Pho*-WT and P49G/G50P species. The T_m values of *Pho*-WT agree with those previously reported by Feio et al. [15]. The melting temperatures of the P49G/G50P mutant are lower than those of *Pho*-WT, and the differences ca. 10 °C larger in the oxidised species than in the reduced ones. In fact, Fig. 3 shows the T_m values of the proteins in this work and Pcs in the literature [17,18]. Clearly, the oxidised forms show a larger variability in their T_m values than the reduced one, suggesting that they are more sensitive to changes in the protein matrix. Opposite, the T_m values of the reduced mutant species are similar to those of *Syn*-WT. The drop in the T_m of the oxidised species is consistent with a decrease in the thermal stability of the oxidised copper site (Fig. SI-1 in Supplementary data). Noteworthy, the oxidised species of mutant P49G/G50P is less thermo-resistant than the reduced, as in *Syn*-WT. Thus, despite this mutation being far away (~20 Å) from the copper centre, the relation between the copper redox state and thermal resistance has been reversed in the mutant, in comparison to *Pho*-WT.

As disruption of the copper site precedes unfolding, we analysed how the P49G/G50P mutation affected it. Tiny differences are observed in the visible region of circular dichroism spectra (see Fig. SI-2). Thus, we resorted to performing XAS spectra of Syn-WT, Pho-WT and P49G/G50P. Full spectra – of both oxidised

Please cite this article in press as: Muñoz-López, F.J., et al. Modulation of copper site properties by remote residues determines the stability of plastocyanins. FEBS Lett. (2010), doi:10.1016/j.febslet.2010.04.013

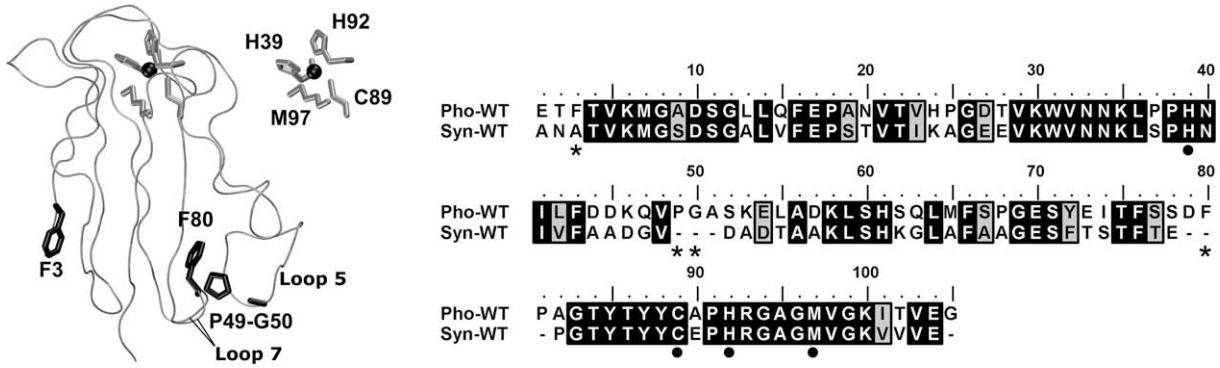

Fig. 1. Structure of Pc from *Phormidium laminosum*. Left: schematic tube representation of backbone coordinates taken from 1baw [31]. Labels mark the residues subjected to mutation, whose side-chains, Cα and N atoms are represented by sticks in black, as well as loops 5 and 7. The structure of the copper site is highlighted on the top right corner. The copper atom is represented as ball in black. Image created with VMD program [32]. Right: Clustal W [36] sequence alignment between *Pho*-WT and *Syn*-WT. Black and grey boxes correspond to identity and similarity between residues, respectively. Asterisks indicate targeted residues in this work. Solid circles label residues binding copper.

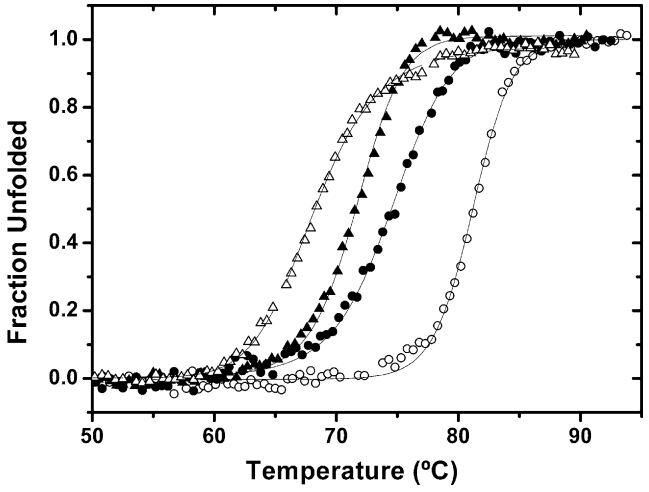

Fig. 2. Thermal denaturation curves of WT and mutant Pc from *Phormidium*. Normalised thermal unfolding curves of the *Pho-WT* (circles) and mutant P49G/G50P (triangles) followed by the fluorescence emission at 350 nm. Open symbols correspond to oxidised species; solid symbols represent data from reduced species.

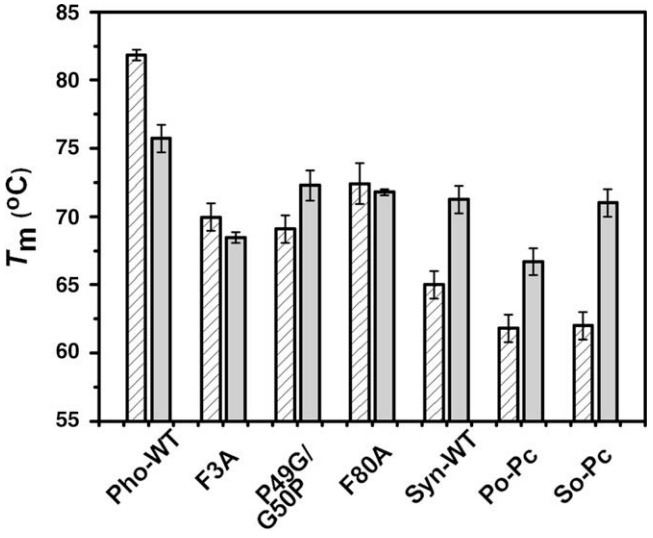

Fig. 3. T_m values for the Pcs from *Phormidium* (*Pho*-WT) and *Synechocystis* (*Syn*-WT) as well as those for the *Phormidium* mutants: F3A, P49G/G50P and F80A. T_m values of plant Pcs (poplar, Po-Pc [17], and spinach, So-Pc [18]) are also shown to allow comparison. Hatched bars represent the oxidised species and grey ones stand for the reduced ones.

and reduced species – are shown in Supplementary data (Fig. SI-3). Fig. 4 displays a comparison between the edge and XANES regions of *Pho*-WT, P49G/G50P, and *Syn*-WT in their oxidised state. The spectra are almost identical (Fig. 4A), except for a feature in the range of energies between 9.014 and 9.060 keV within the XANES region (Fig. 4B), and the edge energies (Fig. 4C).

In *Pho*-WT, the edge shifts 0.6 eV to lower energies with respect to that of Syn-WT. However, the spectra of *Syn*-WT and P49G/G50P Pcs overlap clearly. Although no photo-reduction of the samples was observed along the experiments, we tested this possibility by untuning the monochromator, thereby decreasing the light intensity. No shift of the edge was observed between the experiments (see Fig. SI-3). Hence, the edge shift in *Pho*-WT indicates a difference in the electronic distribution at the copper centre in comparison to the other two Pcs, probably due to a tiny change in the geometry of the metal site. In fact, the spectral shapes and the intensities of the main absorption features in the near-edge region of the XAS spectra are extremely sensitive to changes of the local structure [33]. On the other hand, the spectra corresponding to the reduced forms of the three proteins are identical (Fig. SI-3). As expected, the edges of the reduced forms are shifted to lower

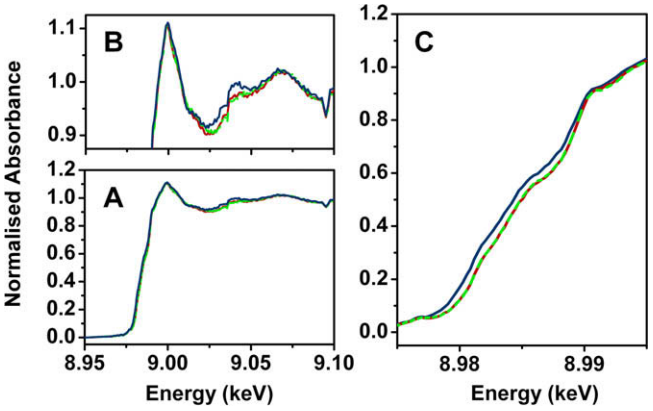

Fig. 4. Edge and XANES region of the X-ray absorption spectra of oxidised *Pho*-WT (blue), P49G/G50P (dashed red) and *Syn*-WT (green) Pcs. (A) Full X-ray absorption spectra. (B) Insight on the XANES region. (C) Details on the edge region. Energy was calibrated by aligning the maximum peak of the first derivative of the reference copper foil spectra that were recorded simultaneously to that of each Pc sample.

Please cite this article in press as: Muñoz-López, F.J., et al. Modulation of copper site properties by remote residues determines the stability of plastocyanins. FEBS Lett. (2010), doi:10.1016/j.febslet.2010.04.013

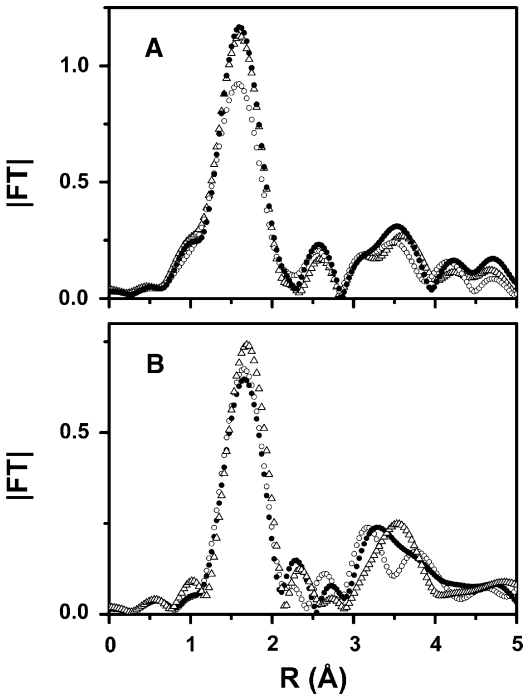

Fig. 5. Modules of the Fourier transforms of Pcs at the Cu K-edge. Open circles, solid circles and triangles correspond to spectra of *Pho*-WT, P49G/G50P and *Syn*-WT, respectively. (A) Oxidised forms and (B) reduced species.

energies by 3.9 eV in Syn-WT and P49G/G50P, and 3.3 eV in Pho-WT.

Contrary to the edge and XANES regions of the absorption spectra, the EXAFS waves of the different samples were very similar – though still depending on their redox state. Fig. 5 shows the Fourier transforms of the k-weighted EXAFS signals for both the oxidised and reduced forms of Pc. The first peak is less intense in oxidised *Pho*-WT than in the others, showing a larger dynamic disorder of the metal site than *Syn*-WT and the P49G/G50P mutant (see Supplementary data for details). Similar to the edge region (Fig. 4), the P49G/G50P mutant resembles *Syn*-WT rather than *Pho*-WT. On the other hand, the reduced forms show only minor differences among them.

4. Discussion

As pointed out before, the redox state of the copper atom affects the thermal stability of Pcs in a different manner, despite them featuring the same copper ligands and surrounding aminoacids. The P49G/G50P mutation reverses the effect of redox state on the T_m despite locating as far as 20 Å from the copper site. It has been reported that charged residues on the protein surface can affect the structure of a type 1 copper site [34,35]. However, mutations herein keep both, the number and the distribution of charges in *Pho*-WT. They do not affect the secondary structure either.

The shift in the XAS edge indicates that the electron density distribution within the oxidised metal site is similar in *Syn*-WT and the P49G/G50P mutant, but different in *Pho*-WT. In addition, the P49G/G50P mutant shows a decrease in the disorder of the first coordination sphere of oxidised copper, according to our XAS data. This indicates that the bond properties of the first coordination sphere of the metal are modulated by remote regions of the protein.

The reduced copper site is insensitive to mutation of remote residues. In fact, XAS spectra are almost identical. Given that unfolding these proteins requires the disruption of the copper site, our XAS data explains the smaller variation of the melting points among the reduced forms of all, WT and mutant species in this work, in comparison to the T_m variability among the oxidised proteins.

The different behaviour of the oxidised and reduced metal species upon mutation contrasts with the absence of a significant change in the macroscopic redox potential of the protein or the secondary structure, as measured by CD. The redox potential relies on the whole system, rather than the copper site alone. For instance, the dynamics at the remote loop containing Pro49 may affect the loops containing the copper site – as their motions are somehow concerted [37] – as well as the entropy of the whole system. Such collective motions could be also responsible for long-range effects of mutations. Further work is needed to clarify this point.

To conclude, this work shows that neutral remote mutations can affect the way the redox state of the metal atom determines the thermal stability of a copper protein. Such long-range effect is not mediated by substantial geometry changes in the metal coordination sphere. However, the higher sensitivity of the oxidised copper site to changes in the protein matrix explains the different behaviour found between *Pho*-WT and *Syn*-WT.

Acknowledgements

This work was supported by the Spanish Ministry of Science and Innovation (MICINN, BFU2006-01361, BFU2009-07190, FIS2-008-03951), the Andalusian Government (BIO-198 and P06-CVI-01713), the ESRF (SC-2486). F.J.M.L. is the recipient of a FPI fellowship (BES-2005-10404) from MICINN. Authors acknowledge Olivier Mathon as local contact of the BM29 beam-line at the ESRF and thank Veronique Mayeux (ESRF) for her collaboration.

Appendix A. Supplementary data

Supplementary data associated with this article can be found, in the online version, at doi:10.1016/j.febslet.2010.04.013.

References

[1] Quevillon-Cheruel, S., Collinet, B., Zhou, C.Z., Minard, P., Blondeau, K., Henkes, G., Aufrère, R., Coutant, J., Guittet, E., Lewit-Bentley, A., Leulliot, N., Ascone, I., Sorel, I., Savarin, P., de La Sierra Gallay, I.L., de la Torre, F., Poupon, A., Fourme, R., Janin, J. and van Tilbeurgh, H. (2003) A structural genomics initiative on yeast proteins. J. Synchrotron Radiat. 10, 4–8.
[2] Robinson, C.R., Liu, Y., Thomson, J.A., Sturtevant, J.M. and Sligar, S.G. (1997) Energetics of heme binding to native and denatured states of cytochrome b562. Biochemistry 36, 16141–16146.
[3] Bertini, I., Cowan, J.A., Luchinat, C., Natarajan, K. and Piccioli, M. (1997) Characterization of a partially unfolded high potential iron protein. Biochemistry 36, 9332–9339.
[4] Leckner, J., Bonander, N., Wittung-Stafshede, P., Malmstrom, B.G. and Karlsson, B.G. (1997) The effect of the metal ion on the folding energetics of azurin: a comparison of the native, zinc and apoprotein. Biochim. Biophys. Acta 1342, 19–27.
[5] Goedken, E.R., Keck, J.L., Berger, J.M. and Marqusee, S. (2000) Divalent metal cofactor binding in the kinetic folding trajectory of Escherichia coli ribonuclease HI. Protein Sci. 9, 1914–1921.
[6] Gough, J. and Chothia, C. (2004) The linked conservation of structure and function in a family of high diversity: the monomeric cupredoxins. Structure 12, 917–925.
[7] Díaz-Quintana, A., Hervás, M., Navarro, J.A. and De la Rosa, M.A. (2008) Plastocyanin and cytochrome c6: the soluble electron carriers between the cytochrome b6f complex and photosystem I in: Structure of Photosynthetic Proteins (Fromme, P., Ed.), pp. 181–200, Wiley-VCH, Weinheim, Germany.
[8] Hervas, M., Navarro, J.A. and De la Rosa, M.A. (2003) Electron transfer between membrane complexes and soluble proteins in photosynthesis. Acc. Chem. Res. 36, 798–805.
[9] Adman, E.T. (1991) Copper protein structures. Adv. Protein Chem. 42, 145–197.
[10] Sykes, A.G. (1991) Plastocyanin and the blue copper proteins. Struct. Bond. 75, 175–224.
[11] Wittung-Stafshede, P. (2004) Role of cofactors in folding of the blue-copper protein azurin. Inorg. Chem. 43, 7926–7933.

[12] Stirpe, A., Sportelli, L. and Guzzi, R. (2006) A comparative investigation of the thermal unfolding of pseudoazurin in the Cu(II)-holo and apo form. Biopolymers 83, 487–497.
[13] Pozdnyakova, I., Guidry, J. and Wittung-Stafshede, P. (2001) Probing copper ligands in denatured *Pseudomonas aeruginosa* azurin: unfolding His117Gly and His46Gly mutants. J. Biol. Inorg. Chem. 6, 182–188.
[14] Alcaraz, L.A. and Donaire, A. (2004) Unfolding process of rusticyanin. Evidence of protein aggregation. Eur. J. Biochem. 271, 4284–4292.
[15] Feio, M.J., Navarro, J.A., Teixeira, M.S., Harrison, D., Karlsson, B.G. and De la Rosa, M.A. (2004) A thermal unfolding study of plastocyanin from the thermophilic cyanobacterium *Phormidium laminosum*. Biochemistry 43, 14784–14791.
[16] Sandberg, A., Harrison, D.J. and Karlsson, B.G. (2003) Thermal denaturation of spinach plastocyanin: effect of copper site oxidation state and molecular oxygen. Biochemistry 42, 10301–10310.
[17] Taneva, S.G., Kaiser, U., Donchev, A.A., Dimitrov, M.I., Mantele, W. and Muga, A. (1999) Redox-induced conformational changes in plastocyanin: An infrared study. Biochemistry 38, 9640–9647.
[18] Gross, E.L., Draheim, J.E., Curtiss, A.S., Crombie, B., Scheffer, A., Pan, B., Chiang, C. and Lopez, A. (1992) Thermal denaturation of plastocyanin: the effect of oxidation state, reductants, and anaerobicity. Arch. Biochem. Biophys. 298, 413–419.
[19] Feio, M.J., Díaz-Quintana, A., Navarro, J.A. and De la Rosa, M.A. (2006) Thermal unfolding of plastocyanin from the mesophilic cyanobacterium *Synechocystis* sp PCC 6803 and comparison with its thermophilic counterpart from *Phormidium laminosum*. Biochemistry 45, 4900–4906.
[20] Varley, J.P.A., Moehrle, J.J., Manasse, R.S., Bendall, D.S. and Howe, C.J. (1995) Characterization of plastocyanin from the cyanobacterium *Phormidium-Laminosum* - copper-inducible expression and SecA-dependent targeting in *Escherichia coli*. Plant Mol. Biol. 27, 179–190.
[21] De la Cerda, B., Navarro, J.A., Hervas, M. and De la Rosa, M.A. (1997) Changes in the reaction mechanism of electron transfer from plastocyanin to photosystem I in the cyanobacterium *Synechocystis sp.* PCC 6803 as induced by site-directed mutagenesis of the copper protein. Biochemistry 36, 10125–10130.
[22] Privalov, P.L. (1979) Stability of proteins: small globular proteins. Adv. Protein Chem. 33, 167–241.
[23] Santoro, M.M. and Bolen, D.W. (1988) Unfolding free energy changes determined by the linear extrapolation method. 1. Unfolding of phenylmethanesulfonyl alpha-chymotrypsin using different denaturants. Biochemistry 27, 8063–8068.
[24] Sinha, A., Yadav, S., Ahmad, R. and Ahmad, F. (2000) A possible origin of differences between calorimetric and equilibrium estimates of stability parameters of proteins. Biochem. J. 345 (Pt 3), 711–717.
[25] Sreerama, N. and Woody, R.W. (2000) Estimation of protein secondary structure from circular dichroism spectra: comparison of CONTIN, SELCON, and CDSSTR methods with an expanded reference set. Anal. Biochem. 287, 252–260.
[26] Ortega, J.M., Hervas, M. and Losada, M. (1988) Redox and acid–base characterization of cytochrome b-559 in photosystem II particles. Eur. J. Biochem. 171, 449–455.
[27] Rehr, J.J., Albers, R.C. and Zabinsky, S.I. (1992) High-order multiple-scattering calculations of X-ray-absorption fine-structure. Phys. Rev. Lett. 69, 3397–3400.
[28] Ravel, B. and Newville, M. (2005) Athena and Artemis: interactive graphical data analysis using Ifeffit. J. Synchrotron Radiat. 12, 537–541.
[29] Newville, M. (2001) IFEFFIT: interactive XAFS analysis and FEFF fitting. J. Synchrotron Radiat. 8, 322–324.
[30] Muñoz-López, F.J., Raugei, S., De la Rosa, M.A., Díaz-Quintana, A. and Carloni, P. (2010) Changes in non-core regions stabilise plastocyanin from the thermophilic cyanobacterium *Phormidium laminosum*. J. Biol. Inorg. Chem. 15, 329–338.
[31] Bond, C.S., Bendall, D.S., Freeman, H.C., Guss, J.M., Howe, C.J., Wagner, M.J. and Wilce, M.C.J. (1999) The structure of plastocyanin from the cyanobacterium *Phormidium laminosum*. Acta Crystallogr. D 55, 414–421.
[32] Humphrey, W., Dalke, A. and Schulten, K. (1996) VMD: visual molecular dynamics. J. Mol. Graph. 14, 33–38.
[33] Chaboy, J. (2009) Relationship between the structural distortion and the Mn electronic state in $La_{1-x}Ca_xMnO_3$: a Mn K -edge XANES study. J. Synchrotron Rad. 16, 533–544.
[34] Sato, K. and Dennison, C. (2002) Effect of histidine 6 protonation on the active site structure and electron-transfer capabilities of pseudoazurin from *Achromobacter cycloclastes*. Biochemistry 41, 120–130.
[35] Harrison, M.D., Yanagisawa, S. and Dennison, C. (2005) Investigating the cause of the alkaline transition of phytocyanins. Biochemistry 44, 3056–3064.
[36] Larkin, M.A., Blackshields, G., Brown, N.P., Chenna, R., McGettigan, P.A., McWilliam, H., Valentin, F., Wallace, I.M., Wilm, A., Lopez, R., Thompson, J.D., Gibson, T.J. and Higgins, D.G. (2007) Clustal W and Clustal X version 2.0. Bioinformatics 23, 2947–2948.
[37] Arcangeli, C., Bizzarri, A.R. and Cannistraro, S. (2001) Concerted motions in copper plastocyanin and azurin: an essential dynamics study. Biophys. Chem. 90, 45–56.

Please cite this article in press as: Muñoz-López, F.J., et al. Modulation of copper site properties by remote residues determines the stability of plastocyanins. FEBS Lett. (2010), doi:10.1016/j.febslet.2010.04.013